

Plasma Knots

Oliver Gross^{a,*}, Ulrich Pinkall^a, Peter Schröder^b

^a*Technische Universität Berlin, Institut für Mathematik, Straße des 17. Juni 136, 10623, Berlin, Germany*
^b*California Institute of Technology, 1200 E. California Blvd., Pasadena, 91125, CA, USA*

Abstract

We present a Lagrangian method for the computation of ideal *plasma knots* and *links*. It is based on a variational principle for stable equilibria of an ideal plasma in the case of a free boundary subjected to external magnetic or plasma pressure forces. For this purpose, we introduce a structure preserving discretization of plasma based on decompositions of Riemannian manifolds representing pressure confined plasma regions in magnetohydrostatic equilibrium. Moreover, we show that, by the virtue of an analogy, the method can be used for the approximation of steady Euler-flows of arbitrarily complex topology.

Keywords: Knot energies, magnetic relaxation, plasma knots, steady Euler-flows

1. Introduction

The search for “natural” representatives for topological spaces is a fundamental task in mathematics. While, the *round sphere* is arguably the undisputed representative for a topological sphere in any dimension, there are no such obvious candidates for most other cases—not even in lower dimensions as for curves and surfaces.

A common approach is to resort to energy functionals that promote desired properties and whose critical points are therefore good substitutes. Well known examples are *elastic curves*, the *Plateau problem*, *minimal surfaces* or *Willmore surfaces*. The corresponding variational energies—the integrated squared curvature of plane curves, the area functional or the integrated mean or squared mean curvature—measure geometric quantities. Less common examples of such energies, which are used in the field of knot theory to find optimal geometric configurations of knots and links, or closed surfaces, are the

Möbius energy [1, 2] or the *tangent-point energy* [3, 4, 5].

Many functionals are inspired by nature: By assigning physical properties to mathematical objects, for example the bending energy is used to model elastic properties of space curves. The *rope length* of *tight knots* [6], is the minimum length of rope—perfectly hard, perfectly flexible and with circular cross section of fixed diameter—that is required to tie a knot of a given type. The center curve of such a rope can be thought of as yet another “natural” representation of this knot type. Thus, there are a number of meaningful motivations that lead to different “natural” representatives.

The present paper is motivated by the process of *magnetic relaxation* [7]. That is, we consider an energy that is usually employed for a variational characterization of special configurations of magnetic fields in the context of plasma physics: A magnetic field B is assumed to be in an ambient fluid with pressure p and governed by the laws of *ideal MHD*, i.e., the field lines are “frozen into the fluid”. The magnetic field B dissipates energy (through some process) and magnetic tension causes the individual field lines to shrink, while the magnetic pressure causes them to evenly distribute (and thus experience some kind of “*magnetic elasticity*”). With the field lines frozen into

*corresponding author

Email addresses: ogross@math.tu-berlin.de (Oliver Gross), pinkall@math.tu-berlin.de (Ulrich Pinkall), ps@caltech.edu (Peter Schröder)

the fluid, the topology of the field is preserved throughout the process and topological obstructions (or confining ambient pressure) eventually bring the process to a halt [8, 9, 10, 11].

By a suitable discretization of the plasma into filaments this physically motivated picture constitutes an energy on the space of curves with thickness and thus can also be used for knots and links. A geometric interpretation then gives rise to a computational method to compute such equilibrium configurations.

1.1. Computational Methods

As with the Willmore functional or the rope length problem, precise mathematical statements about minimizers are generally scarce. Consequently, the development of numerical methods to approximate or visually represent such natural representatives has been an active area of research [12, 13, 14, 5, 4].

Relevant numerical methods for magnetic relaxation include so called *magneto-frictional methods* [15, 16, 17, 18, 19, 20]. For surveys on these methods see e.g., [9], [21] or [22].

In particular, a numerical treatment of magnetic relaxation while constraining the topology or allowing for free-boundaries involves considerable computational difficulties [23].

The similarity of ideal magnetic relaxation and the rope length problem—both require an isotopy class preserving tightening process [24]—lead to algorithms from knot theory [12, 13] being used in the magnetic context to approximate the spectra of knotted flux tubes [25, 26], although additional (geometrically more rigid) assumptions were required which neglect magnetic elasticity. Nonetheless, these Lagrangian methods elegantly deal with topology preservation and free-boundary conditions. Other methods that have made relevant progress include [27], [28], [20] and [29].

1.2. Objective

Building on recent work by Padilla et al. [29], we develop and discretize decompositions of Riemannian manifolds representing pressure bounded plasma regions in general magnetohydrostatic equilibrium. We provide corresponding variational principles allowing for free boundary surfaces in the sense of Dixon et al. [23]—including cases of non-ideal MHD.

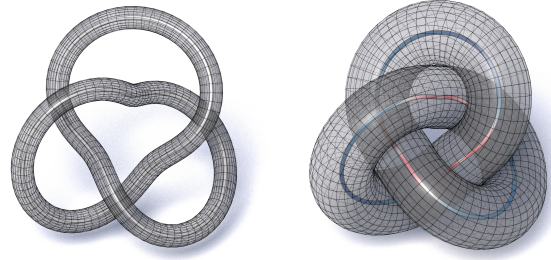


Figure 1: A flux tube in the shape of a trefoil knot (left) and a “*relaxed state*” of the same knot (right) representing a stationary point of the magnetohydrostatic energy.

Moreover, we show how the algorithmic framework provided by Padilla et al. [29] can be extended to compute these more general decompositions. The presented discretization is structure preserving [30] and, in contrast to previous state of the art algorithms, allows for (time-)variable field strength of the discretized plasma filaments and non-vanishing gas pressure on the support of the magnetic field. We demonstrate the applicability of the method on applications proposed by Moffatt [8, 31].

2. Magnetic Relaxation

With pioneering work by Moffatt [8, 31], magnetic relaxation has established itself as an independent area of research, with influence ranging from plasma physics and classical fluid dynamics to purely mathematical disciplines such as differential geometry, differential topology and knot theory [32, 33, 34, 35, 10, 7, 36].

2.1. Steady Euler-Flows

Based on the process of ideal magnetic relaxation [8] formally introduced stationary points that are *topologically accessible* from a given field B . For a precise definition of topological accessibility we refer the reader to Moffatt’s original work. For now, we can imagine that we are dealing with a limit of ideal relaxation, which may not necessarily share the same topology as the original field, but can experience discontinuities across so called *current sheets* (cf. Fig. 5).

By drawing analogies between magnetic fields and ordinary fluids as

$$\begin{aligned} B &\longleftrightarrow u \\ \operatorname{curl} B &\longleftrightarrow \omega \\ p &\longleftrightarrow h_0 - h \end{aligned}$$

where u is the fluid velocity, ω the fluid vorticity, h_0 a constant and h the Bernoulli pressure, his result also implies the existence of a steady Euler-flow that is topologically accessible from any given Euler-flow of arbitrarily complex topology [9, Sec 3.1].

2.2. The Energy of Knots and Links

Moffatt [31] proposed another interesting application of ideal magnetic relaxation in the field of knot theory. He considered the equilibria of essentially knotted flux tubes resulting from the process of ideal magnetic relaxation, and suggested that the spectrum of relaxed state energies of an essentially knotted flux tube is a topological invariant capturing the complexity of the knot type. Special cases of the problem were studied by [37], whereas Maggioni and Ricca [25, 26] studied the problem from a geometric point of view. In particular, Ricca and Maggioni [38] found similarities between the ground-state energy spectra of magnetic knots and links and the bending energy of tight knots and links, both of which are physically motivated.

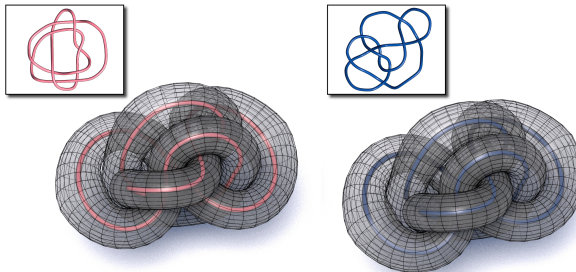


Figure 2: Relaxing the *Perko pair* (insets) is considered to be a benchmark for numerical algorithms aiming to find *ideal* conformations of prime knots. The respective configurations resulting from our method are shown side-by-side.

3. Ideal Magnetohydrostatics

In physics, a variety of simplifications are used in the description of static solutions of ideal MHD. It is known that the resulting equations are the Euler-Lagrange equations of corresponding variational principles for the magnetic energy which differ in the imposed constraints or boundary conditions. In this section we briefly review the customary principles, before we extend all cases to pressure confined free-boundary conditions in the sense of Dixon et al. [23] in Sec. 5 for the ideal case and Sec. 8.1 for more general cases.

We consider a three-dimensional Riemannian manifold M with *magnetic field* $B \in \Gamma TM$, $\operatorname{div} B = 0$ and *pressure* $p \in C^\infty(M)$. If not stated differently, we assume that the field is confined by a *magnetic surface*, i.e., $\langle B, N \rangle = 0$ where N is the normal vector of ∂M .

In the absence of gravity, a magnetic field B is said to be in *magnetohydrostatic equilibrium* if it satisfies the *ideal magnetohydrostatics* (MHS) equation

$$(\operatorname{curl} B) \times B = \operatorname{grad} p. \quad (1)$$

When studying strong magnetic fields or fields in a vacuum, the *low-beta* limit can be employed [39], which neglects pressure effects and for which Eq. (1) reduces to the so called *force-free* condition

$$(\operatorname{curl} B) \times B = 0. \quad (2)$$

Solutions to (2) are referred to as *force-free* fields, whose curl is co-linear to the original field, i.e., $\operatorname{curl} B = \lambda B$ for some smooth function $\lambda \in C^\infty(M)$. If the scalar function λ is constant, the corresponding field is called *linear force-free* and another important special case of (linear) force-free fields is given by *harmonic fields* which satisfy $\operatorname{curl} B = 0$.

Distinguished by the imposed boundary conditions and constraints, the simplifications of Eq. (1) emerge as the Euler-Lagrange equations of the total potential energy

$$\mathcal{E}(B, p) = \mathcal{B}(B) + \mathcal{P}(p) \quad (3)$$

where

$$\mathcal{B}(B) = \frac{1}{2} \int_M |B|^2 \det \quad \text{and} \quad \mathcal{P}(p) = \int_M p \det \quad (4)$$

are the *magnetic energy* respectively the *internal energy*.

In the process of magnetic relaxation, the field is physically transported by a perfectly conducting fluid with vanishing resistivity. The induction equation of ideal MHD implies that the field is “frozen” into the fluid, i.e., the isotopy class of the field B is preserved. Therefore, we consider variations of the field B of the form

$$\dot{B} = \operatorname{curl}(Y \times B), \quad (5)$$

where $Y \in \Gamma TM$ is the variational vector field of a family of diffeomorphisms $t \mapsto \varphi_t: M \rightarrow M$, $t \in (-\epsilon, \epsilon)$ on M .

In the low-beta limit, the variational formulation of the general magnetohydrostatic case (Eq. (1), [40]) is known as the *minimum energy theorem for force-free fields* [39, Sec. 2.8]. In Sec. 8.1 we will also discuss generalized variational principles for linear force-free and harmonic fields, which require variations which are incompatible with ideal MHD and therefore require special treatment.

4. Magnetohydrostatic Bubbles

Ultimately we are interested in equilibrium configurations of magnetic fields which are bound by a flux surface and confined by an ambient pressure, though the geometry is not held fixed. Eq. (1) states that in magnetohydrostatic equilibrium, the pressure is constant along the field lines of the field B . Moreover, the pressure is constant away from the magnetic field and has jumps across the bounding flux surface. It is therefore natural to decompose the manifold M into the support of the magnetic field and its complement and consider plasma configurations which restrict to smooth configurations on those regions.

Definition 4.1. A plasma bubble configuration on a Riemannian manifold M consists of a decomposition of M into finitely many manifolds with corners M_i , $M = M_0 \cup M_1 \cup \dots \cup M_n$ with $M_i^\circ \cap M_j^\circ = \emptyset$, divergence-free vector fields $B_i \in \Gamma TM_i$ tangent to non-empty interfaces $\Sigma_{ij} := \partial M_i \cap \partial M_j$, $0 < j \neq i$ and pressure functions $p_i \in C^\infty(M_i)$ such that $0 \leq p_i|_{\Sigma_{i0}} < p_0|_{\Sigma_{i0}}$ and $dp_i(B_i) = 0$. In particular, $M_B = M_1 \cup \dots \cup M_n$.

We define the *magnetic field* $B \in \Gamma TM_B$ of the plasma

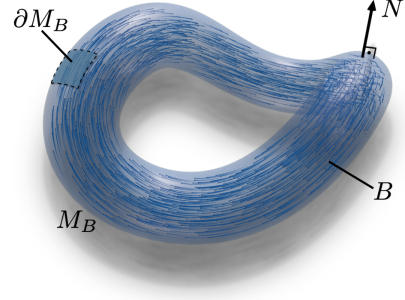


Figure 3: An isolated flux tube is an example of a plasma bubble configuration.

bubble configuration as

$$B(x) := \begin{cases} B_i(x) & \text{if } x \in M_i, \\ 0 & \text{if } x \in M_0^\circ. \end{cases} \quad (6)$$

and similarly the *interior pressure* $p^B \in C^\infty(M_B)$ as

$$p^B(x) := \begin{cases} p_i(x) & \text{if } x \in M_i, \\ 0 & \text{if } x \in M_0^\circ. \end{cases} \quad (7)$$

Loosely speaking, a plasma bubble configurations is a decomposition of M into two regions—a *flux domain* M_B , which carries the magnetic field and (possibly) some gas, and a *gas domain* M_0 , which contains only gas but no magnetic field. In Appendix A we prove

Proposition 4.2. *The magnetic field of a plasma bubble configuration is weakly divergence-free.*

Remark 4.3. For the special case that $p^B = 0$ vanishes everywhere such domain decompositions, to which we will refer to as *magnetic bubble configurations*, were already considered by Dixon et al. [23] and Padilla et al. [29].

Such a configuration is called a *magnetohydrostatic configuration* if it weakly satisfies the magnetohydrostatic equation. In Appendix B we proof conditions for when this is the case and which are summarized in

Theorem 4.4. *A plasma bubble configuration $p_0 > 0$, $p^B \in C^\infty(M_B)$, $B \in \Gamma TM$, weakly satisfies the magnetohydrostatic equation if and only if*

1. p_0 is piecewise constant,

2. $(\operatorname{curl} B) \times B = \operatorname{grad} p^B$,
3. $p_0 = p^B + \frac{|B|^2}{2}$ on $\partial M_0 \cap \partial M_B$.

In particular, the second condition tells us that the fields B_i are in magnetohydrostatic equilibrium on their respective supports (cf. Eq. (1)).

5. A Variational Principle for Magnetohydrostatic Plasma Bubble Configurations

In this section we will extend the variational principles with pressure confined free-boundary conditions to the general case of magnetic fields in magnetohydrostatic equilibrium.

The work needed to create a bubble M_B with interior pressure $p^B \geq 0$ in an ambient pressure p_0 is

$$\int_{M_B} (p_0 - p^B) \det, \quad (8)$$

and we denote the *pressure difference* between interior and ambient pressures by

$$p^\Delta := p_0 - p^B. \quad (9)$$

We view the exterior pressure as an additional structure on the manifold M and therefore denote the ambient Riemannian manifold as a triple $(M, \langle \cdot, \cdot \rangle, p_0)$, whereas a plasma bubble configuration is a triple (M_B, p^B, B) .

Definition 5.1. Let (M_B, p^B, B) be a plasma bubble configuration in a three-dimensional oriented Riemannian manifold $(M, \langle \cdot, \cdot \rangle, p_0)$. Then the *magnetohydrostatic energy* is given by

$$\mathcal{E}(M_B, p^B, B) = \int_{M_B} \left(p^\Delta + \frac{|B|^2}{2} \right) \det. \quad (10)$$

In order to examine the critical points of (10) we compute its variational gradient. When we allow the support $M_B := \operatorname{supp}(B) \subseteq M$ of the field B to change its shape, the *internal energy* of the system

$$\mathcal{P}(M_B, p^B, B) = \int_{M_B} p^\Delta \det \quad (11)$$

changes.

Theorem 5.2. Let (M_B, p^B, B) be a plasma bubble configuration in a three-dimensional oriented Riemannian manifold $(M, \langle \cdot, \cdot \rangle, p_0)$ and $N \in \Gamma TM$ be the outward-pointing normal of ∂M_B . Then the energy variation corresponding to a variational vector field $Y \in \Gamma TM$ on M is given by

$$\begin{aligned} \mathring{\mathcal{E}}(M_B, p^B, B) &= \int_{M_B} \langle \operatorname{grad} p^\Delta - (\operatorname{curl} B) \times B, Y \rangle \det \\ &\quad + \int_{\partial M_B} \left(p^\Delta - \frac{|B|^2}{2} \right) \langle Y, N \rangle \iota_N \det \\ &\quad + \int_{\partial M_B} \langle B, Y \rangle \langle B, N \rangle \iota_N \det. \end{aligned} \quad (12)$$

Proof. See App. Appendix C. \square

An immediate observation is that the last summand of Eq. (12) vanishes for fields confined by a magnetic surface, i.e., $\langle B, N \rangle = 0$. Therefore, as a direct consequence of Thm. 5.2, we obtain:

Theorem 5.3. Let (M_B, p^B, B) be a plasma bubble configuration in a three-dimensional oriented Riemannian manifold $(M, \langle \cdot, \cdot \rangle, p_0)$. Then the magnetic field B on M_B is a critical point of (10) under variations by diffeomorphisms if and only if B is in magnetohydrostatic equilibrium, i.e., $(\operatorname{curl} B) \times B = \operatorname{grad} p^\Delta$ on its support and $p^\Delta = \frac{|B|^2}{2}$ on $\partial M_0 \cap \partial M_B$.

For vanishing interior pressure $p^B = 0$, this result generalizes a version of the *minimum energy theorem for force-free fields* [39, Sec. 2.8] for pressure confined fields which are bounded by a magnetic surface.

Corollary 5.4. Let (M_B, B) be a magnetic bubble configuration in a three-dimensional oriented Riemannian manifold $(M, \langle \cdot, \cdot \rangle, p_0)$. Then the magnetic field B on M_B is a critical point of (10) under variations by diffeomorphisms if and only if B is in magnetohydrostatic equilibrium, i.e., $(\operatorname{curl} B) \times B = 0$ on its support and $p_0 = \frac{|B|^2}{2}$ on $\partial M_0 \cap \partial M_B$.

6. Discrete Ideal Magnetic Relaxation

Ideal magnetic relaxation as proposed by Moffatt [8] assumes volume preservation in order to account for gas pressure. Considering the gaseous nature of e.g., stellar plasma, this assumption may be deemed unnatural. Thm. 5.2 provides an alternative variational principle

which circumvents this shortcoming, yet still exhibits solutions to Eq. (1) as its critical points. In particular, for an algorithmic treatment, dropping the incompressibility assumption is favorable as no additional pressure projection steps are needed and the discretization of magnetic bubble configurations as introduced by Padilla et al. [29] can be extended to serve as a structure preserving discretization of plasma bubble configurations.

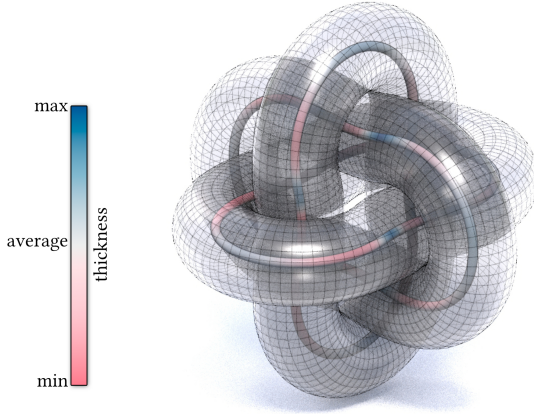


Figure 4: The output of our method for flux tubes in the configuration of Borromean rings. The center curves are colored according to the thickness of the tube indicating that a variable thickness is indeed needed to accurately represent equilibria of the energy in Eq. (10).

6.1. Plasma Filaments

Consider a magnetic flux tube supported on a regular tubular neighborhood with circular cross-section. In this case, we have a well-defined *center curve* $\gamma: [0, L] \rightarrow M$ and we can view the flux domain as a curve with thickness. That is, a pair (γ, A) consisting of a smooth, regular center curve $\gamma: [0, L] \rightarrow M$ together with a *cross-sectional area function* $A: [0, L] \rightarrow \mathbb{R}_{>0}$.

The flux $h > 0$ through every cross section is constant along the center curve and does not change under deformation by orientation preserving diffeomorphisms $\varphi: M \rightarrow M$. Following Padilla et al. [29] we will refer to a curve with thickness (γ, A) together with a fixed flux $h > 0$ as a *magnetic filament* with magnetic field strength associated to tube geometry. Moreover, we employ their

approximation [29, Sec. 5.1] which relates the modulus $|B|$ of a magnetic field to the geometry of (γ, A) .

By allowing for interior gas pressure, we generalize the notion of magnetic filaments and define *plasma filaments* to be curves with thickness with a fixed flux $h > 0$ and an interior pressure $p^B \geq 0$, which, by virtue of (1), is constant along each plasma filament.

Accounting for interior pressure the magnetic field strength associated to a tube geometry confined by an ambient pressure $p_0 > 0$ is determined by

$$\frac{|B|^2}{2} = p^\Delta, \quad (13)$$

which can be derived by following the derivation of Padilla et al. [29, Sec. 5.1] almost verbatim. As expected, this is equivalent to the pressure continuity

$$\frac{|B|^2}{2} + p^B = p_0 \quad (14)$$

across the boundary $\partial M_0 \cap \partial M_B$.

6.2. Discrete Energy and Approximation of the Plasma Domain

For a plasma filament the energy (10) can be computed as

$$\mathcal{E}(\gamma, |B|) = h \int_0^L \left(\frac{p^\Delta}{|B|} + \frac{|B|}{2} \right) ds \quad (15)$$

which approximates $\mathcal{E}(M_B, B)$ where M_B is the plasma filament [29]. A plasma domain M_B is then approximated by a collection Γ of plasma filaments, each representing a fixed flux. Therefore, we may approximate the volumetric energy (10) by the *discrete energy*

$$\mathcal{E}(\Gamma) = \sum_{\gamma \in \Gamma} h \int_0^{L_\gamma} \left(\frac{p^\Delta_\gamma}{|B_\gamma|} + \frac{|B_\gamma|}{2} \right) ds. \quad (16)$$

6.3. Structure Preservation

A number of properties of plasma are preserved under variations by a family of diffeomorphisms $t \mapsto \varphi_t: M \rightarrow M$. The helicity, a measure of the complexity of the magnetic field, is one of them as can be easily shown in the smooth setting. In the discretized setting, by the Lagrangian nature of the algorithm, the isotopy class of the field is preserved (sufficiently small time-stepping provided (Appendix E)) and therefore also the helicity.

In the smooth setup, the magnetic flux $\beta := \iota_B \det$ is transported under diffeomorphisms by $\beta_t = \varphi_t^* \beta_0$. A similar statement holds true for the interior pressure functions. Eq. (1) says that the interior pressure is constant along the field lines, a property which is also preserved under transport by diffeomorphisms.

In the discretized setting, we prescribe a magnetic flux and an interior pressure per filament. Therefore, the property that the gradient of the pressure perpendicular to the field lines (Eq. (1)) is trivially satisfied at all times. Moreover, as we move the curves as Lagrangian variables, these prescribed magnetic fluxes and interior pressures are transported together with the curves and hence remain constant along the curves, i.e. the field lines of the magnetic field B .



Figure 5: The initialized configuration (left) and the relaxed state (middle) of a Hopf link discretized by 100 plasma filaments per link component together with a cross-section of the relaxed state (right).



Figure 6: Consecutive stages of the evolution (left to right) of discrete ideal magnetic relaxation of a variety of knots and links: trefoil knot, figure eight knot, torus knot $T_{5,2}$, whitehead link, borromean rings, two linked trefoil knots (top to bottom).

7. Numerical Experiments

We performed numerical experiments on the discrete ideal magnetic relaxation presented in Sec. 6. For our experiments we use the code provided by Padilla et al. [29] which we adapted according to the discussions presented in Sec. 5 and Sec. 6, leaving the methods for the energy minimization unchanged (cf. Sec. Appendix E).

7.1. Knots and Links

We were able to successfully relax a variety of knots and links (Fig. 6). Pierański [12] states that “any algorithm aimed at finding the ideal conformations of prime knots should pass is the ability to bring knots 10_{161} and 10_{162} , the Perko pair, to a single, ideal conformation.” We successfully performed a corresponding experiment whose outcome is shown in Fig. 2. Another such experiment considers the torus knots $T_{2,3}$ and $T_{3,2}$ [31], which

our algorithm relaxes to the same equilibrium configuration (Fig. 1 and Fig. 6 first row).

A key improvement our formulation in terms of plasma filaments brings (compared to algorithms for relaxation from knot theory) is that it allows for filaments with variable, time-dependent thickness—thus capturing the phenomenon of magnetic elasticity (cf. Sec. 1.1). Fig. 4 showcases equilibrium states of Eq. (16) which exhibit a non-constant thickness along their center curve, so that this feature is indeed needed for faithful experiments.

7.2. Approximation of Steady Euler-Flows

By choosing to represent the field topology by a larger collection of field lines, we believe that the method is a useful tool for approximating steady Euler-flows of arbitrarily complex topology. Comparing the relaxed states of

Fig. 4 or Fig. 1 to Fig. 7, it is clear that the approximation of the knots and links with only a single flux strand per link component is markedly coarse. With many filaments per connected components, the results are thought to be much closer to a “physical ground truth” as the free-boundary conditions affect the equilibrium states to a larger extent.



Figure 7: The initialized configurations (left column) and the relaxed states (right column) of a trefoil knot discretized by 100 plasma filaments (top row) and borromean rings discretized by 50 plasma filaments per link component (bottom row).

From Fig. 5 it is apparent, that the resulting equilibrium configurations share the characteristic structures that the smooth counterparts have. For example, the filaments at the outer edge are approximately of the same thickness, representing a uniform field strength matching the pressure continuity conditions (cf. Thm. 4.4). The same is true for the current sheets, which in our model are accounted for by the surfaces of the plasma filaments. That said, Fig. 5 shows that the model also automatically handles the formation of these current sheets which are found in our model as the contacting surfaces of the plasma filaments. The resulting configuration appears to be close to the geometrically less flexible discretization employed by Hudson et al. [28].

The field lines of a generic magnetic field in MHS equilibrium do not have to be closed [10, Chapter 2], so that we unfortunately cannot apply our discretization in those

cases. This problem shares similarities with the Clebsch representation of vorticity lines of fluid fields [41]. Chern et al. [41] point out that by the Poincaré recurrence theorem [42], almost every such field line will return arbitrarily closely to its initial point, making it “almost closed” still allowing for meaningful approximations with our method.

8. Variational Principles for Non-Ideal Relaxation with Free-Boundary Conditions

For many practical applications, the magnetic field is not bounded by a magnetic surface, but field lines pass through the boundary ∂M . One such example is the solar corona, where the domain of interest is the exterior of the sun bounded by the sun’s photosphere [23, 43, 29]. The corresponding boundary conditions which fix the isotopy class of the field in this case are commonly referred to as *line tied*. The variational principle for magnetohydrostatic plasma bubbles still applies, provided we only consider diffeomorphisms $M \rightarrow M$ which fix the boundary $\Sigma := \partial M$ pointwise.

Theorem 8.1. *Let (M_B, p^B, B) be a plasma bubble configuration in a three-dimensional oriented Riemannian manifold $(M, \langle \cdot, \cdot \rangle, p_0)$ with boundary Σ . Then the magnetic field B on M_B is a critical point of (10) under variations which fix the boundary Σ pointwise if and only if B is in magnetohydrostatic equilibrium, i.e., $(\operatorname{curl} B) \times B = \operatorname{grad} p^\Delta$ on its support and $p^\Delta = \frac{|B|^2}{2}$ on $\partial M_0 \cap \partial M_B$.*

Moreover, we retrieve the main result of Padilla et al. [29, Thm 3.] as a corollary of Thm. 8.1 for the special case of magnetic bubble configurations ($p^B = 0$).

Corollary 8.2. *Let (M_B, B) be a magnetic bubble configuration in a three-dimensional oriented Riemannian manifold $(M, \langle \cdot, \cdot \rangle, p_0)$ with boundary $\partial M = \Sigma$. Then the magnetic field B on M_B is a critical point of (10) under variations which fix the boundary Σ pointwise if and only if B is force-free on its support and $p_0 = \frac{|B|^2}{2}$ on $\partial M_0 \cap \partial M_B$.*

8.1. Non-Ideal Cases

So called *Taylor relaxation* constrains the (*relative*) helicity [32, 44], which can be understood as the degree of knottedness of the field, together with flux boundary conditions. Interestingly, constraining the helicity does not

suffice to preserve the field topology—which is incompatible with ideal MHD—and stationary points of the corresponding variational principle are linear force-free fields on their support [23].

So if M is a manifold with boundary, the appropriate class of variations comes from diffeomorphisms $M \rightarrow M$ which do not leave the boundary fixed, but only respect prescribed boundary conditions on $\Sigma_B := \Sigma \cap M_B$. By considering this class of variations, we also obtain statements for the missing cases we discussed in Sec. 3 with free-boundary conditions. The generalization of the *Woltjer minimum-energy principle* presented by Dixon et al. [23] can be stated as

Theorem 8.3. *Let (M_B, B) be a magnetic bubble configuration in a three-dimensional oriented Riemannian manifold $(M, \langle \cdot, \cdot \rangle, p)$ with boundary $\partial M = \Sigma$. Then if the magnetic field B on M_B is a critical point of (10) under variations which fix the intersections $\Sigma_B = \partial M \cap M_B$, the boundary flux $\Phi \in C^\infty(\Sigma)$ and the relative helicity, the magnetic field is linear force-free, i.e., $\operatorname{curl} B = \lambda B$ for a constant λ .*

In case we also drop the helicity constraint, harmonic fields arise from the least restrictive class of variations we consider, which consists of those diffeomorphisms $M \rightarrow M$ whose restrictions to ∂M solely preserve the boundary conditions. The corresponding variational principle is known as the *minimum energy theorem for potential fields* [39, Sec. 2.8]. The following Lemma from Padilla et al. [29] states that being *curl-free* on Σ is already a sufficient condition for critical points of (10) to be harmonic.

Lemma 8.4. *Let (M_B, B) be a magnetic bubble configuration in a three-dimensional oriented Riemannian manifold $(M, \langle \cdot, \cdot \rangle, p_0)$ with boundary $\partial M = \Sigma$ and the set of field lines which have points on the boundary is dense in M_B . Then if B is force-free and $\operatorname{curl} B = 0$ on Σ_B , then B is harmonic.*

The result does not come by surprise, as divergence-free and force-free property of B imply that there is a $\lambda \in C^\infty(M_B)$ such that $\operatorname{curl} B = \lambda B$ from which we conclude that $0 = \langle \operatorname{grad} \lambda, B \rangle$, i.e., λ is constant along each field line. Hence, if $\lambda = 0$ on the boundary, it vanishes along the whole field line.

Theorem 8.5. *Let (M_B, B) be a magnetic bubble configuration in a three-dimensional oriented Riemannian manifold $(M, \langle \cdot, \cdot \rangle, p_0)$ with boundary $\partial M = \Sigma$. Moreover, let $\langle B, N \rangle(p) \neq 0$ for all $p \in \Sigma$, and the sets $\{p \in \Sigma \mid B^T \neq 0\}$ be dense in Σ and $\{p \in M_B \mid \text{the integral curve of } B \text{ through } p \text{ hits } \partial M\}$ be dense in M_B . Then if the magnetic field B on M_B is a critical point of (10) under variations which fix the intersections $\Sigma_B = \partial M \cap M_B$ and the boundary flux $\Phi \in C^\infty(\Sigma)$, the magnetic field is curl-free, i.e., $\operatorname{curl} B = 0$.*

Proof. See App. Appendix D □

There exist a variety of efficient numerical methods for computing harmonic fields from given boundary conditions, even on infinite domains [45, 46].

9. Discussion and Concluding Remarks

Inspired by the thought experiment of magnetic relaxation, we have derived a comprehensive collection of variational principles for special static solutions of ideal MHD with pressure confined free-boundary conditions which complement results obtained in [23] and [29].

Moreover, we present a corresponding structure preserving discretization of plasma bubble configurations into plasma filaments as a straightforward generalization of the results obtained by Padilla et al. [29] which allows us to employ their numerical framework—coming with the same benefits and limitations.

Though basic experiments were successful (cf. Sec. 7.1), starting from generic initial configurations one cannot yet expect to find true global minima with the local nature of the present algorithmic framework. The strictly local nature of the quasi-Newton method for energy minimization proposed in [29] is prone to getting stuck in local minima. For a more efficient energy minimization which is likely to attain global minima, a more elaborate optimization (as performed e.g., in [4]) is needed.

Plasma filaments can be thought of as curves with thickness and thus, similar as for the rope length problem, the resulting configurations may be considered “natural” representatives of the given knot or link type. The respective spectrum of ground state energies is believed to provide information about the topological complexity, although a suitable normalization would be necessary.

In particular the inclusion of filaments with a variable thickness makes the presented framework less geometrically rigid and thus favorable (compared to algorithms developed for the rope length problem) for the relaxation of knots and links by magnetic relaxation.

Another interesting extension would be to include reconnection mechanisms of filaments and boundary treatments which is necessary for possible physical applications such as simulations of superfluids [47, 48, 49] or non-ideal relaxation which is of importance for solar physics, or controlled fusion reactors [33, 50, 51, 52].

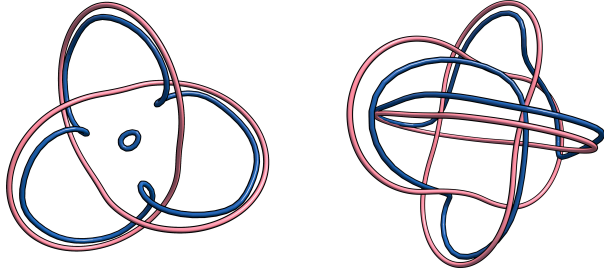


Figure 8: Plasma filaments (blue) resulting from smoothing a \mathbb{C}^2 -valued wave function ψ which was obtained from isotopy constrained plasma filaments in magnetohydrostatic equilibrium (red) using the method by Chern et al. [41]. We note that smoothing the wave function ψ leads to reconnections and thus a change of the filament topology.

A first way to approach this task could be, for example, to complement the method presented here with another method based on Clebsch variables [48, 41]. Based on level sets, Clebsch variables allow an implicit (yet Lagrangian) representation of the plasma filaments which can naturally handle topology changes resulting from reconnection. Since all our filaments represent the same magnetic flux, we can construct a \mathbb{C}^2 -valued wave function ψ from them. If we smooth the function ψ and reconstruct the filaments represented by it, reconnections take place in a natural way (Fig. 8).

Though this approach leads to reconnections (Fig. 8), it fails to capture the helicity preservation that is sought for in many applications. The plasma filaments we propose in this paper inherently assume untwisted magnetic fields and are thus cannot account for the twist resulting from helicity preserving reconnection of, e.g., a Hopf link as in Fig. 9 [53, 47, 49].

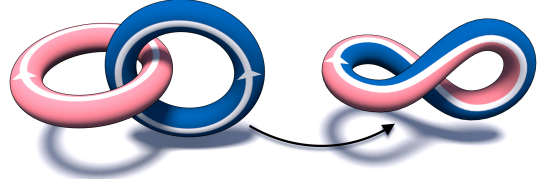


Figure 9: Accounting for weak resistivity, helicity preserving relaxation of a Hopf link consisting of two unknotted, linked components each carrying an untwisted field with flux $h > 0$ leads to a reconnection in such a way that the two tubes become a single, twisted tube carrying flux h .

Acknowledgements

This work was funded by the Deutsche Forschungsgemeinschaft (DFG - German Research Foundation) - Project-ID 195170736 - TRR109 "Discretization in Geometry and Dynamics", the Caltech Center for Information Science & Technology, and the Einstein Foundation Berlin. Additional support was provided by SideFX software.

References

- [1] M. H. Freedman, Z.-X. He, Z. Wang, Möbius energy of knots and unknots, *Ann. of Math.* 139 (1994) 1.
- [2] R. B. Kusner, J. M. Sullivan, Möbius-invariant knot energies, in: A. Stasiak, V. Katritch, L. H. Kauffman (Eds.), *Ideal knots*, volume 19, World Scientific Publishing Company, 1998, pp. 315–352.
- [3] O. Gonzalez, J. H. Maddocks, Global curvature, thickness, and the ideal shapes of knots, *Proc. Nat. Acad. Sci.* 96 (1999) 4769–4773.
- [4] C. Yu, H. Schumacher, K. Crane, Repulsive Curves, *ACM Trans. Graph.* 40 (2021) 268:1–268:19.
- [5] C. Yu, C. Brakensiek, H. Schumacher, K. Crane, Repulsive surfaces, *ACM Trans. Graph.* 40 (2021).
- [6] L. H. Kauffman, *Knots and Applications*, K. & E. series on knots and everything, World Scientific, 1995.
- [7] H. K. Moffatt, Helicity and singular structures in fluid dynamics, *Proc. Nat. Acad. Sci.* 111 (2014) 3663–3670.

- [8] H. Moffatt, Magnetostatic equilibria and analogous euler flows of arbitrarily complex topology. part 1. fundamentals, *J. Fl. Mech.* 159 (1985) 359–378.
- [9] H. K. Moffatt, Relaxation under topological constraints, in: H. K. Moffatt, G. M. Zaslavsky, P. Comte, M. Tabor (Eds.), *Topological Aspects of the Dynamics of Fluids and Plasmas*, Springer, 1992, pp. 3–28.
- [10] V. I. Arnold, B. A. Khesin, *Topological methods in hydrodynamics*, volume 125 of *Applied Mathematical Sciences*, Springer, 2008.
- [11] A. R. Yeates, Magnetohydrodynamic relaxation theory, in: D. MacTaggart, A. Hillier (Eds.), *Topics in Magnetohydrodynamic Topology, Reconnection and Stability Theory*, Springer International Publishing, 2020, pp. 117–143.
- [12] P. Pierański, In search of ideal knots, 1998.
- [13] T. Ashton, J. Cantarella, M. Piatek, E. J. Rawdon, Knot tightening by constrained gradient descent, *Experiment. Math.* 20 (2011) 57–90.
- [14] Y. Soliman, A. Chern, O. Diamanti, F. Knöppel, U. Pinkall, P. Schröder, Constrained Willmore Surfaces, *ACM Trans. Graph.* 40 (2021).
- [15] R. Chodura, A. Schlüter, A 3D code for MHD Equilibrium and Stability, *J. Comput. Phys.* 41 (1981) 68–88.
- [16] W. H. Yang, P. A. Sturrock, S. K. Antiochos, Force-free magnetic fields—the magneto-frictional method, *Astrophys. J.* 309 (1986) 383–391.
- [17] J. A. Klimchuk, P. A. Sturrock, Three-dimensional force-free magnetic fields and flare energy buildup, *Astrophys. J.* 385 (1992) 344–353.
- [18] G. Roumeliotis, P. A. Sturrock, S.-K. Antiochos, A numerical study of the sudden eruption of sheared magnetic fields, *Astrophys. J.* 423 (1994) 847.
- [19] A. N. McClymont, L. Jiao, Z. Mikić, Problems and progress in computing three-dimensional coronal active region magnetic fields from boundary data, *Sol. Phys.* 174 (1997) 191–218.
- [20] C. B. Smiet, S. Candelaresi, D. Bouwmeester, Ideal relaxation of the Hopf fibration, *Phys. Plasmas.* 24 (2017) 072110.
- [21] Y. Guo, C. Xia, R. Keppens, G. Valori, Magneto-frictional modeling of coronal nonlinear force-free fields. I. Testing with analytic solutions, *Astrophys. J.* 828 (2016) 82.
- [22] A. R. Yeates, On the limitations of magneto-frictional relaxation, *Geophys. Astrophys. Fluid Dyn.* 116 (2022) 305–320.
- [23] A. M. Dixon, M. A. Berger, E. R. Priest, P. K. Browning, A generalization of the woltjer minimum-energy principle, *Astron. Astrophys.* 225 (1989) 156.
- [24] J. Cantarella, R. B. Kusner, J. M. Sullivan, On the minimum ropelength of knots and links, *Invent. Math.* 150 (2002) 257–286.
- [25] F. Maggioni, R. L. Ricca, On the groundstate energy of tight knots, *Proc. R. Soc. Lond. A* 465 (2009) 2761–2783.
- [26] R. L. Ricca, F. Maggioni, On the groundstate energy spectrum of magnetic knots and links, *J. Phys. A: Math. Theor.* 47 (2014) 205501.
- [27] C. E. DeForest, C. C. Kankelborg, Fluxon Modeling of Low-Beta Plasmas, *J. Atmos. Sol.-Terr. Phys.* 69 (2007) 116–128.
- [28] S. R. Hudson, R. L. Dewar, G. Dennis, M. J. Hole, M. McGann, G. von Nessi, S. Lazerson, Computation of multi-region relaxed magnetohydrodynamic equilibria, *Phys. Plasmas.* 19 (2012) 112502.
- [29] M. Padilla, O. Gross, F. Knöppel, A. Chern, U. Pinkall, P. Schröder, Filament Based Plasma, *ACM Trans. Graph.* 41 (2022) 153:1–153:14.
- [30] K. Crane (Ed.), *An Excursion Through Discrete Differential Geometry*, volume 76, American Mathematical Society, 2020.
- [31] H. K. Moffatt, The energy spectrum of knots and links, *Nature* 347 (1990) 367–369.

- [32] H. K. Moffatt, The degree of knottedness of tangled vortex lines, *J. Fl. Mech.* 35 (1969) 117–129.
- [33] J. Cantarella, Topological structure of stable plasma flows, University of Pennsylvania, 1999. Phd Thesis.
- [34] W. K. Schief, Hidden integrability in ideal magnetohydrodynamics: The pohlmeier-lund-regge model, *Phys. Plasmas.* 10 (2003) 2677–2685.
- [35] W. K. Schief, Nested toroidal flux surfaces in magnetohydrostatics. generation via soliton theory, *J. Plasma Phys.* 69 (2003) 465–484.
- [36] A. R. Yeates, G. Hornig, A complete topological invariant for braided magnetic fields, *Journal of Physics: Conference Series* 544 (2014) 012002.
- [37] A. Y. K. Chui, H. K. Moffatt, Minimum energy magnetic fields with toroidal topology, in: H. K. Moffatt, G. M. Zaslavsky, P. Comte, M. Tabor (Eds.), *Topological Aspects of the Dynamics of Fluids and Plasmas*, Springer, 1992, pp. 195–218.
- [38] R. L. Ricca, F. Maggioni, Groundstate energy spectra of knots and links: magnetic versus bending energy, in: P. Reiter, S. Blatt, A. Schikorra (Eds.), *New Directions in Geometric and Applied Knot Theory*, 2017, pp. 276–288.
- [39] E. R. Priest, *Magnetohydrodynamics of the Sun*, Cam. U. P., 2014.
- [40] P. C. Kendall, The Variational Formulation of the Magneto-Hydrostatic Equations, *Astrophys. J.* 131 (1960) 681.
- [41] A. Chern, F. Knöppel, U. Pinkall, P. Schröder, Inside Fluids: Clebsch Maps for Visualization and Processing, *ACM Trans. Graph.* 36 (2017).
- [42] H. Poincaré, Sur les équations de la dynamique et le probleme des trois corps, *Acta Math.* 13 (1890) 270.
- [43] A. R. Yeates, T. Amari, I. Contopoulos, X. Feng, D. H. Mackay, Z. Mikić, T. Wiegmann, J. Hutton, C. A. Lowder, H. Morgan, et al., Global Non-Potential Magnetic Models of the Solar Corona During the March 2015 Eclipse, *Space Sci. Rev.* 214 (2018) 99.
- [44] M. A. Berger, Introduction to magnetic helicity, *Plasma Physics and Controlled Fusion* 41 (1999) B167.
- [45] D. Stansby, A. R. Yeates, S. T. Badman, pfsspy: A Python Package for Potential Field Source Surface Modelling, *J. Open Source Softw.* 5 (2020) 2732.
- [46] M. S. Nabizadeh, R. Ramamoorthi, A. Chern, Kelvin transformations for simulations on infinite domains, *ACM Trans. Graph.* 40 (2021) 97:1–97:15.
- [47] M. W. Scheeler, D. Kleckner, D. Proment, G. L. Kindlmann, W. T. Irvine, Helicity conservation in topology-changing reconnections: the flow of linking and coiling across scales, *ArXiv e-prints* 1404 (2014).
- [48] A. Chern, F. Knöppel, U. Pinkall, P. Schröder, S. Weißmann, Schrödinger’s smoke, *ACM Trans. Graph.* 35 (2016).
- [49] E. Priest, D. Longcope, The creation of twist by reconnection of flux tubes, *Solar Physics* 295 (2020) 48.
- [50] S. R. Hudson, E. Startsev, E. Feibush, A new class of magnetic confinement device in the shape of a knot, *Phys. Plasmas.* 21 (2014) 010705.
- [51] P. M. Bellan, *Magnetic Helicity, Spheromaks, Solar Corona Loops, And Astrophysical Jets*, World Scientific Publishing Company, 2018.
- [52] P. M. Bellan, Caltech Lab Experiments and the Insights They Provide Into Solar Corona Phenomena, *J. Geophys. Res.* 125 (2020) e2020JA028139.
- [53] H. K. Moffatt, Some remarks on topological fluid mechanics, in: R. L. Ricca (Ed.), *An introduction to the geometry and topology of fluid flows*, Springer, 2001, pp. 3–10.
- [54] M. Reddiger, B. Poirier, On the Differentiation Lemma and the Reynolds Transport Theorem for Manifolds with Corners, 2020. [arXiv:1906.03330](https://arxiv.org/abs/1906.03330).

Appendix A. Proof of Thm. 4.2

for $i \neq j$, using Stokes' theorem we compute

Proof. Let $M_i^\varepsilon = \{x \in M_i \mid \text{dist}(x, \partial M_i) > \varepsilon\}$. Then there is a smooth function $\varphi_i: M \rightarrow [0, 1]$ such that $\text{supp } \varphi_i \subset M_i$ and $\varphi_i(x) = 1$ for all $x \in M_i^\varepsilon$. Define $\tilde{B} = \sum_{i>0} \varphi_i B_i$ and let $\phi \in C^\infty(M)$ be compactly supported away from ∂M . Then, since φ_i, B_i have disjoint supports from φ_j, B_j for $i \neq j$, using Stokes' theorem and the divergence-free property of the B_i fields, we compute

$$\begin{aligned} & \int_M \phi \operatorname{div}(\tilde{B}) \det \\ &= \sum_{i>0} \int_M (\operatorname{div}(\phi \varphi_i B_i) - \varphi_i \langle \operatorname{grad} \phi, B_i \rangle) \det \\ &\equiv - \sum_{i>0} \int_{M_i} \langle \operatorname{grad} \phi, B_i \rangle \det \\ &= - \sum_{i>0} \int_{M_i} \operatorname{div}(\phi B_i) \det \\ &= - \sum_{i>0} \int_{\partial M_i} \phi \langle B_i, N_i \rangle \det \\ &= 0, \end{aligned}$$

where we used that the normal vectors N_i of ∂M_i and B_i are perpendicular, $N_i \perp B_i|_{\partial M_i}$, and \equiv denotes equality up to terms vanishing for $\varepsilon \rightarrow 0$. \square

$$\begin{aligned} & \int_M \langle (\operatorname{curl} \tilde{B}) \times \tilde{B}, Y \rangle \det \\ &= \sum_{i>0} \int_M \varphi_i^2 \langle (\operatorname{curl} B) \times B, Y \rangle \det \\ &\quad + \sum_{i>0} \int_M \langle \operatorname{grad} \varphi_i^2, \langle Y, B_i \rangle B_i - |B_i|^2 Y \rangle \det \\ &= \sum_{i>0} \int_M \varphi_i^2 \langle (\operatorname{curl} B) \times B, Y \rangle \det \\ &\quad + \sum_{i>0} \int_M \frac{1}{2} \operatorname{div} (\langle Y, B_i \rangle B_i - |B_i|^2 Y) \det \\ &= \sum_{i>0} \int_M \varphi_i^2 \langle (\operatorname{curl} B) \times B, Y \rangle \det \\ &\quad + \sum_{i>0} \int_M \frac{1}{2} \varphi_i^2 \operatorname{div} (|B_i|^2 Y) \det \\ &\equiv \sum_{i>0} \int_{M_i} \langle (\operatorname{curl} B) \times B, Y \rangle \det \\ &\quad + \sum_{i>0} \int_{\partial M_i} \frac{|B_i|^2}{2} \langle Y, N_i \rangle \iota_{N_i} \det \end{aligned}$$

where we used that the normal vectors N_i of ∂M_i and B_i are perpendicular, $N_i \perp B_i|_{\partial M_i}$, and \equiv denotes equality up to terms vanishing for $\varepsilon \rightarrow 0$.

Moreover, again by Stokes' theorem, we have

Appendix B. Proof of Thm. 4.4

Proof. Let $M_i^\varepsilon = \{x \in M_i \mid \text{dist}(x, \partial M_i) > \varepsilon\}$. Then there is a smooth function $\varphi_i: M \rightarrow [0, 1]$ such that $\text{supp } \varphi_i \subset M_i$ and $\varphi_i(x) = 1$ for all $x \in M_i^\varepsilon$. Define

$$\tilde{p} = \varphi_0 p, \quad \tilde{B} = \sum_{i>0} \varphi_i B_i, \quad \tilde{p}^B = \sum_{i>0} \varphi_i p_i.$$

Now, let $Y \in \Gamma TM$ be compactly supported away from ∂M . Then, since φ_i, B_i have disjoint supports from φ_j, B_j

$$\begin{aligned} & \int_M \langle \operatorname{grad} \tilde{p}_i, Y \rangle \det \\ &= \sum_{i>0} \int_M (\langle \operatorname{grad} \varphi_i, p_i Y \rangle + \varphi_i \langle \operatorname{grad} p_i, Y \rangle) \det \\ &= - \sum_{i>0} \int_M \varphi_i \operatorname{div}(p_i Y) \det + \sum_{i>0} \int_M \varphi_i \langle \operatorname{grad} p_i, Y \rangle \det \\ &\equiv - \sum_{i>0} \int_{M_i} \operatorname{div}(p_i Y) \det + \sum_{i>0} \int_{M_i} \langle \operatorname{grad} p_i, Y \rangle \det \\ &= - \sum_{i>0} \int_{\partial M_i} p_i \langle Y, N_i \rangle \iota_{N_i} \det + \sum_{i>0} \int_{M_i} \langle \operatorname{grad} p_i, Y \rangle \det \end{aligned}$$

and similarly

$$\begin{aligned}\int_M \langle \operatorname{grad} \tilde{p}_0, Y \rangle \det &= - \int_{\partial M_0} p_0 \langle Y, N_0 \rangle \det \\ &\quad + \int_{M_0} \langle \operatorname{grad} p_0, Y \rangle \det.\end{aligned}$$

We thus obtain

$$\begin{aligned}&\int_M \langle \operatorname{curl} \tilde{B} \times \tilde{B} - \operatorname{grad} \tilde{p}_0 - \operatorname{grad} \tilde{p}^B, Y \rangle \det \\ &\equiv \sum_{i>0} \left(\int_{M_i} \langle (\operatorname{curl} B) \times B - \operatorname{grad} p_i, Y \rangle \det \right. \\ &\quad \left. + \int_{M_0} \langle \operatorname{grad} p_0, Y \rangle \det \right) \\ &\quad + \sum_{i,j>0} \int_{\partial M_i \cap \partial M_j} \left[\left(p_i + \frac{|B_i|^2}{2} \right) - \left(p_j + \frac{|B_j|^2}{2} \right) \right] \langle Y, N_0 \rangle \iota_{N_0} \det \\ &\quad + \sum_{i>0} \int_{\partial M_0 \cap \partial M_i} \left[p_0 - \left(p_i + \frac{|B_i|^2}{2} \right) \right] \langle Y, N_0 \rangle \iota_{N_0} \det\end{aligned}$$

which vanishes for all Y if and only if $(\operatorname{curl} B) \times B = \operatorname{grad} p_i$, $\operatorname{grad} p_0 = 0$, $p_i + \frac{|B_i|^2}{2} = p_0$ on $\partial M_0 \cap \partial M_i$ for $i > 0$ and $\frac{|B_i|^2}{2} = \frac{|B_j|^2}{2}$ on $\partial M_i \cap \partial M_j$ for $i, j > 0$. \square

Appendix C. Proof of Thm. 5.2

Applying the *Reynolds transport theorem* [54] to the time-dependent terms $p^\Delta, \frac{|B|^2}{2}$ we get

$$\begin{aligned}\frac{d}{dt} \Big|_{t=0} \int_{M_B} \varphi_t^*(p^\Delta \det) &= \int_{M_B} \langle \operatorname{grad} p^\Delta, Y \rangle \det \\ &\quad + \int_{\partial M_B} p^\Delta \langle Y, N \rangle \iota_N \det,\end{aligned}$$

$$\begin{aligned}\frac{d}{dt} \Big|_{t=0} \int_{M_B} \varphi_t^* \left(\frac{|B|^2}{2} \det \right) &= \int_{M_B} \langle \mathring{B}, B \rangle \det \\ &\quad + \int_{\partial M_B} \frac{|B|^2}{2} \langle Y, N \rangle \iota_N \det,\end{aligned}$$

where we used Cartan's magic formula, integration by parts and the Divergence theorem.

Moreover, with $\mathring{B} = \operatorname{curl}(Y \times B)$, we compute

$$\begin{aligned}&\int_{M_B} \langle \mathring{B}, B \rangle \det \\ &= \int_{M_B} \langle \operatorname{curl}(Y \times B), B \rangle \det \\ &= \int_{M_B} \langle Y \times B, \operatorname{curl} B \rangle \det \\ &\quad - \int_{M_B} \operatorname{div}(|B|^2 Y - \langle B, Y \rangle B) \det \\ &= - \int_{M_B} \langle \operatorname{curl} B \times B, Y \rangle \det \\ &\quad - \int_{\partial M_B} \left(|B|^2 \langle Y, N \rangle - \langle B, Y \rangle \langle B, N \rangle \right) \iota_N \det,\end{aligned}$$

so that the claim follows by putting everything together and sorting the terms.

Appendix D. Proof of Thm. 8.5

To prove the theorem we will use

Lemma Appendix D.1. *Let M be a three-dimensional, compact Riemannian manifold with boundary $\partial M = \Sigma$ and $X \in \Gamma TM$. Then*

$$(\operatorname{curl} X)^T = \operatorname{curl} X^T,$$

where $(\cdot)^T$ denotes the restriction to $\Gamma T\Sigma$.

Now we are in a position to show the actual statement:

Proof of Thm. 8.5. We will write $\det_\Sigma := \iota_N \det$ for the induced volume form on Σ and add subscripts $(\cdot)_\Sigma$ to vector calculus operators corresponding to Σ . Then by the assumption and similar computations as needed for Thm. 8.2,

$$0 = \int_\Sigma \langle Y, \langle B, N \rangle B \rangle \det_\Sigma$$

for all $Y \in \Gamma T\Sigma$ with

$$\begin{aligned}0 &= \mathcal{L}_Y (\langle B, N \rangle \det_\Sigma) \\ &= (\langle Y, \operatorname{grad} \langle B, N \rangle \rangle + \langle B, N \rangle \operatorname{div}_\Sigma(Y)) \det_\Sigma \\ &= \operatorname{div}_\Sigma (\langle B, N \rangle Y) \det_\Sigma.\end{aligned}$$

Hence, for all $\tilde{Y} \in \Gamma T\Sigma$ with $\text{div}_\Sigma(\tilde{Y}) = 0$, we have

$$0 = \int_\Sigma \left\langle \frac{1}{\langle B, N \rangle} \tilde{Y}, \langle B, N \rangle B \right\rangle \det_\Sigma = \int_\Sigma \langle \tilde{Y}, B \rangle \det_\Sigma,$$

which implies the existence of a function $\phi \in C^\infty(\Sigma)$ such that $\text{grad}_\Sigma \phi = B^T$. By Lem. Appendix D.1 we thus have that on Σ

$$(\text{curl } B)^T = \text{curl } B^T = \text{curl grad}_\Sigma \phi = 0.$$

By Thm. 8.2, criticality implies force-freeness, so that by decomposing $\text{curl } B$ and B into their tangential and normal components, we have

$$\begin{aligned} 0 &= ((\text{curl } B) \times B) \Big|_\Sigma \\ &= (\text{curl } B)^T \times \langle B, N \rangle B \\ &\quad + \langle \text{curl } B, N \rangle N \times B^T + (\text{curl } B)^T \times B^T, \end{aligned}$$

which implies $\langle \text{curl } B, N \rangle = 0$ as $(\text{curl } B)^T = 0$ and $N \times B^T \neq 0$ on a dense set. Thus $\text{curl } B|_\Sigma = 0$ and the statement follows from Lem. 8.5. \square

Appendix E. Numerical Energy Minimization

For our numerical experiments we have adapted the codebase provided by [29] according to the discussions presented in Sec. 5 and Sec. 6. In this section we outline the implementation of the resulting algorithm.

Eq. (16) provides an approximation of the magnetohydrostatic energy (10) expressed in terms of the energies (15) of a discrete set of plasma filaments Γ . Following [29], we interpret the filament wise energy (15) as the length of the respective plasma filament $\gamma \in \Gamma$ measured in a conformally changed metric

$$d\tilde{s} := e^u ds = \begin{cases} \sqrt{2p^\Delta} ds & \text{in } M_0 \\ \left(\frac{p_\gamma^\Delta}{|B_\gamma|} + \frac{|B_\gamma|}{2} \right) ds & \text{in } M_B, \end{cases} \quad (\text{E.1})$$

which is smooth in M_0 and M_B respectively and continuous across $\partial M_0 \cap \partial M_B$. Therefore, for optimization of the energy can be performed by iteratively shortening the length of the individual filaments with respect to $d\tilde{s}$.

Appendix E.1. Time-Splitting

We note that the metric $d\tilde{s}$ depends on $|B|$ which is determined from the geometry of the plasma filaments Γ . We circumvent the coupled nature of the optimization problem by introducing the following time splitting, which was first proposed by [29]: First, given a configuration Γ of plasma filaments, the associated magnitude of a magnetic field $|B|$ and hence the conformal factor is computed. Then, fixing the conformal factor, a curve-shortening flow step is performed. To find a fixed point, these two steps are alternated until convergence.

Algorithm 1

Input: Initial curve set Γ , ambient pressure $p_0 > 0$, interior pressure $p^B \geq 0$.

Output: Γ in relaxed state.

- 1: **while** not converged **do**
- 2: $u, \text{grad } u \leftarrow \text{COMPUTEMETRIC}(\Gamma)$;
- 3: $\Gamma \leftarrow \text{CURVESHORTENING}(\Gamma)$;
- 4: **end while**

Appendix E.2. Implementation

We have implemented our proposed algorithm in *SideFX*' *Houdini* where we represent the individual plasma filaments as a *discrete curve*, i.e., a map $\gamma: \{0, \dots, n\} \rightarrow \mathbb{R}^3$, where the position of a vertex $i \in \{0, \dots, n\}$ is denoted by γ_i . Due to the fixed flux and $h = |B|A$, the magnitude $|B_i|$ of the associated magnetic field at vertex i is determined by the radius r of the plasma filament [29, Sec. 6]. For all our experiments shown we have chosen $p_0 = 1$ and p^Δ constant across all filaments. The remaining parameter $h > 0$ then amounts to a scaling of the resulting equilibrium configurations.

Therefore, given the collection Γ of discretized plasma filaments, we may compute the logarithmic conformal factors

$$u_i = \log \left(\frac{p_i^\Delta}{|B_i|} + \frac{|B_i|}{2} \right)$$

for every vertex i . The gradient of the logarithmic conformal factor u_i is approximated employing a finite difference scheme

$$(\text{grad } u)_i \approx \sum_{\gamma_j \in \mathcal{N}(\gamma_i)} (u_j - u_i) \frac{\gamma_j - \gamma_i}{|\gamma_j - \gamma_i|^2},$$

where $\mathcal{N}(\gamma_i)$ is a set of neighboring vertices of γ_i including vertices coming from virtual filaments that fill the gas domain with field strength according to (13). Note that for the gradient approximation we only merely need to know how to evaluate the logarithmic conformal factor u on the discrete curves γ .

For the curve-shortening flow (with respect to $d\tilde{s}$) we perform a quasi-Newton step proposed by [29] which, denoting the k -th iterate of γ_i by γ_i^k , is given by

$$\gamma_i^{k+1} = w_+ \gamma_{i+1}^k + w_- \gamma_{i-1}^k - \frac{1}{2} (w_- \ell_-^2 + w_+ \ell_+^2) (\text{grad } u)(\gamma_i^k),$$

where $\ell_- := |\gamma_i^k - \gamma_{i-1}^k|$, $\ell_+ := |\gamma_{i+1}^k - \gamma_i^k|$ and

$$w_- := \frac{\ell_+ e^{u(\gamma_{i-1}^k)}}{\ell_+ e^{u(\gamma_{i-1}^k)} + \ell_- e^{u(\gamma_{i+1}^k)}}, \quad w_+ := \frac{\ell_- e^{u(\gamma_{i+1}^k)}}{\ell_+ e^{u(\gamma_{i-1}^k)} + \ell_- e^{u(\gamma_{i+1}^k)}}.$$

In order to preserve the field topology, we bound the step size by the tube radius of the plasma filaments.